Submitted to the
**International Conference on High Energy Physics**
**16-22 August 2004, Beijing, China**

**Abstract: 5-0263** **Session: QCD hard interactions**

# An NLO QCD analysis of inclusive cross-section data and jet production data from the ZEUS experiment at HERA-I

ZEUS Collaboration

**Abstract**

The ZEUS inclusive differential cross-section data from HERA-I, for charged and neutral current processes taken with $e^+$ and $e^-$ beams, have been used in a new NLO QCD analysis to extract the parton distribution functions of the proton. The precision of the high-$x$ gluon determination is improved by using ZEUS differential cross-section data on inclusive jet production in $e^+p$ scattering and di-jet production in $\gamma p$ scattering. The additional information from jet production data also allows an accurate extraction of $\alpha_s(M_Z^2)$ at NLO,

$$\alpha_s(M_Z^2) = 0.1183 \pm 0.0028(\text{exp}) \pm 0.0008(\text{model}).$$

# 1 Introduction

ZEUS data from HERA-I on neutral and charged current (NC and CC) $e^+p$ and $e^-p$ cross-sections [1–6] have been used in a NLO QCD DGLAP [7–10] analysis in order to determine the parton distributions functions (PDFs) using data from within a single experiment. The PDFs are usually determined in global fits [11–14], which use fixed target DIS data as well as HERA data. In such analyses, the high statistics HERA NC $e^+p$ data, which span the range $6.3 \times 10^{-5} < x < 0.65,\ 2.7 < Q^2 < 30,000$ GeV$^2$, have determined the low-$x$ sea and gluon distributions, whereas the fixed target data have determined the valence distributions and the higher-$x$ sea and gluon distributions. The most important inputs for determining the valence distributions have been the $\nu$-Fe and the $\mu D$ fixed target data, but these data sets suffer from uncertainties due to heavy target corrections [15]. In the present analysis the ZEUS high $Q^2$ cross-section data [2–6] are used to determine the valence distributions thus eliminating such uncertainties.

PDF fits to DIS data alone have suffered from a lack of information on the high-$x$ gluon because the gluon PDF contributes only indirectly to the inclusive DIS cross-sections. However it makes a direct contribution to jet cross-sections through the Boson-Gluon-Fusion process. In the present analysis ZEUS measured jet cross sections, in the DIS and photoproduction regimes, are used to constrain the mid to high-$x$ gluon PDF and to extract the value of $\alpha_s(M_Z^2)$.

The PDFs are presented with full accounting for uncertainties from correlated systematic errors (as well as from statistical and uncorrelated sources). Performing an analysis within a single experiment has considerable advantages in this respect, since the global fits have found significant tensions between different data sets, which make a rigorous statistical treatment of uncertainties difficult.

# 2 Analysis

The kinematics of lepton hadron scattering is described in terms of the variables $Q^2$, the invariant mass of the exchanged vector boson, Bjorken $x$, the fraction of the momentum of the incoming nucleon taken by the struck quark (in the quark-parton model), and $y$ which measures the energy transfer between the lepton and hadron systems. The differential cross-section for the NC process is given in terms of the structure functions by

$$\frac{d^2\sigma(e^\pm p)}{dxdQ^2} = \frac{2\pi\alpha^2}{Q^4 x}\left[Y_+\, F_2(x,Q^2) - y^2\, F_L(x,Q^2) \mp Y_-\, xF_3(x,Q^2)\right],$$

where $Y_\pm = 1 \pm (1-y)^2$. The structure functions $F_2$ and $xF_3$ are directly related to quark distributions, and their $Q^2$ dependence, or scaling violation, is predicted by perturbative

QCD. At $Q^2 \lesssim 1000$ GeV$^2$ $F_2$ dominates the charged lepton-hadron cross-section and for $x \lesssim 10^{-2}$, $F_2$ itself is sea quark dominated whereas its $Q^2$ evolution is controlled by the gluon contribution, such that ZEUS data provide crucial information on quark and gluon distributions. At high $Q^2$, the structure function $xF_3$ becomes increasingly important, and gives information on valence quark distributions. The CC interactions enable separation of the flavour of the valence distributions at high $x$, since their (LO) cross-sections are given by,

$$\frac{d^2\sigma(e^+p)}{dxdQ^2} = \frac{G_F^2 M_W^4}{(Q^2+M_W^2)^2 2\pi x} x\left[(\bar{u}+\bar{c}) + (1-y)^2(d+s)\right],$$

$$\frac{d^2\sigma(e^-p)}{dxdQ^2} = \frac{G_F^2 M_W^4}{(Q^2+M_W^2)^2 2\pi x} x\left[(u+c) + (1-y)^2(\bar{d}+\bar{s})\right].$$

The present analysis is performed within the conventional paradigm of leading twist, NLO QCD, with the renormalisation and factorization scales chosen to be $Q^2$. The QCD predictions for the structure functions are obtained by solving the DGLAP evolution equations at NLO in the $\overline{\mathrm{MS}}$ scheme. These equations yield the PDFs at all values of $Q^2$ provided they are input as functions of $x$ at some input scale $Q_0^2$. The resulting PDFs are then convoluted with coefficient functions, to give the structure functions which enter into the expressions for the cross-sections. These coefficient functions are calculated using the general mass variable flavour number scheme of Roberts and Thorne [16] for heavy quark production. For a full explanation of the relationships between DIS cross-sections, structure functions, PDFs and the QCD improved parton model see, for example, ref. [17].

The PDFs for $u$ valence, $d$ valence, total sea, gluon and the difference between the $d$ and $u$ contributions to the sea, are each parametrized by the form

$$p_1 x^{p_2}(1-x)^{p_3}(1+p_4 x)$$

at $Q_0^2 = 7$ GeV$^2$. No advantage in $\chi^2$ results from using more complex polynomial forms. The flavour structure of the light quark sea allows for the violation of the Gottfried sum rule, but since there is no information on the shape of the $\bar{d}-\bar{u}$ distribution in a fit to ZEUS data alone this distribution has its shape fixed consistent with the Drell-Yan data [18] and its normalisation consistent with the size of the Gottfried sum-rule violation [19,20]. A suppression of the strange sea of a factor of 2 at $Q_0^2$, is also imposed consistent with neutrino induced dimuon data from CCFR [21]. The fit is not sensitive to reasonable variation of these assumptions.

Parameters are further restricted as follows. The normalisation parameters $p_1$ for the $d$ and $u$ valence and for the gluon are constrained to impose the number sum-rules and momentum sum-rule. The $p_2$ parameter which constrains the low-$x$ behaviour of the $u$ and $d$ valence distributions is set equal, since there is no information to constrain any difference. When fitting to ZEUS inclusive cross-section data alone it is also necessary to constrain some of the parameters which control the high-$x$ sea and gluon shapes, because HERA-I data do not have high statistics at large-$x$, in the region where these distributions are small. There are two possible strategies towards making these constraints.

Firstly, the focus is on the valence distributions and the number of free parameters describing the high-$x$ sea and gluon is restricted. There are various ways to make restrictions. One possibility is to set $p_4 = 0$ for both these distributions. However this does not allow any structure at medium $x$ for $Q^2$ near the input scale. Alternatively, the $p_4$ parameters can be freed but the $p_3$ parameters fixed to the values obtained in the ZEUS global fit [14]. In this case, model uncertainties on the high-$x$ sea and gluon PDFs must include the effect of changing these fixed values of $p_3$ within the limits of their errors as determined in the global fit. In practice there is very little difference in the shapes and errors on the sea and gluon PDFs determined by these two ways of making restrictions. Distributions are presented for the latter choice. This fit is called the ZEUS-O fit.

Secondly, a more ambitious strategy is pursued. ZEUS data on jet production are included in the PDF fit. This not only gives more information on the high-$x$ gluon PDF, but also establishes that NLO QCD is able to simultaneously describe inclusive cross-sections and jet cross-sections providing a compelling test of QCD factorization. This fit is called the ZEUS-JETS fit. The method of incorporating the jet production data in the fit is discussed in detail in Sec. 3.2.

The strong coupling constant is fixed to $\alpha_s(M_Z^2) = 0.118$ [22], for both the ZEUS-O and the ZEUS-JETS fit. The value of $\alpha_s(M_Z^2)$ and the gluon shape are correlated through the DGLAP equations. The extra constraint which the jet production data gives on the gluon PDF can also be exploited to make an accurate determination of $\alpha_s(M_Z^2)$, which accounts for this correlation, by making a simultaneous fit for $\alpha_s(M_Z^2)$ and the PDF parameters. This is called the ZEUS-JETS-$\alpha_s$ fit.

For all analyses the following cuts are made on the data: (i) $W^2 > 20$ GeV$^2$ to reduce the sensitivity to target mass and higher twist contributions which become important at high $x$ and low $Q^2$; (ii) $Q^2 > 2.5$ GeV$^2$ to remain in the kinematic region where perturbative QCD should be applicable. Full account has been taken of correlated experimental systematic errors by the Offset Method, as decribed in the previous ZEUS analysis [14] and discussed extensively in [23, 24].

# 3 Results

## 3.1 ZEUS-O fit results

The ZEUS-O fit is made to ZEUS inclusive cross-section data from a total luminosity of 112 $\text{pb}^{-1}$ of HERA-I running. There are 10 free parameters describing the input PDF distributions, 33 sources of systematic correlated error and 4 different normalisations for the data sets. The fit $\chi^2$ is 376 for 509 data points. A good description of cross-section data over the whole range of $Q^2$ from 2.5 to 30000 $\text{GeV}^2$ is obtained. The quality of the fit to the high-$Q^2$ reduced cross-section data is illustrated in Fig. 1.

The valence distributions are shown in Fig 2. Although the high-$x$ valence distributions are not quite as well constrained as they are in global fits including fixed target data [11–14] they are becoming competitive, particularly for the less well known $d$-valence distribution. Furthermore, they are free from uncertain heavy target corrections.

The gluon and sea distributions are shown in Fig. 3. They exhibit the familiar features of the sea rising at low $x$ down to surprisingly low-$Q^2$ values, and the gluon flattening and then becoming valence-like in the same kinematic region. They are as well determined as the corresponding distributions of the global fits [11–14] at low $x$, since the ZEUS data were crucial in determining these distributions for all the fits. At high $x$ they have the same uncertainties as the global fits because of the constraints that have been applied.

The experimental errors represent the most significant source of uncertainty on these distributions. Variation of analysis choices, such as the value of $Q_0^2$, the minimum $Q^2$ of data entering the fit, and changing the form of the parametrization at $Q_0^2$, do not produce a large model uncertainty.

## 3.2 ZEUS-JETS fit results

In the ZEUS-JETS fit, the inclusive cross-section data are supplemented by two sets of ZEUS jet cross-section data, which give constraints on the gluon distribution in the range $0.01 \lesssim x \lesssim 0.1$. These data sets are

- 30 data points from six DIS inclusive jet differential cross-sections as a function of the transverse energy in the Breit frame, $E_T^B$, for different $Q^2$ bins [25],
- 38 data points from six direct photoproduction di-jet cross-sections as a function of the transverse energy in the laboratory frame of the most energetic jet, $E_T^{jet1}$, for different jet pseudo-rapidity ranges [26].

For each of these data sets the calorimeter energy scale uncertainty and the normalization uncertainty have been treated as correlated systematic errors.

The programme of Frixione and Ridolfi [27] is used to compute NLO QCD cross sections for photoproduced di-jets and DISENT [28] is used to compute NLO QCD cross sections for jet production in DIS. These programmes are too slow to be used every iteration of a fit. Thus these codes are used to produce grids, in $\xi$ (the parton momentum fraction) and $\mu_F^2$ (the factorization scale), of weights which represent sub-process cross-sections for each flavour of parton (gluon, up-type, down-type). This is done for each cross-section bin and these weights are then used to reconstruct the cross-sections as follows

$$d\sigma(jets) = \sum_n \sum_{a=u,d,g} \int \int d\xi d\mu_F^2 f_a(\xi, \mu_F^2) \alpha_s^n(\mu_R) \sigma_a^n(\xi, \mu_F^2) \tag{1}$$

where $f_a$ is the PDF for parton type $a$ at parton momentum fraction $\xi$ and scale $\mu_F$, and $\sigma_a^n$ is the sub-process cross-section weight for the $n$-th order contribution to the cross-section. The factorization scale is chosen as $\mu_F = Q$ for the DIS jets, and the renormalization scale is $\mu_R = E_T^B$ (with $\mu_R = Q$ as a cross-check). For the photoproduced di-jets the standard scale choices are $\mu_R = \mu_F = E_T/2$ (where $E_T$ is the summed transverse momentum of final state partons). The grids reproduce the NLO predictions to better than 0.5%. The predictions are then multiplied by hadronization corrections before they are fitted to data. The predictions for DIS jet production are also multiplied by $Z^0$ corrections.

The predictions for photoproduced jets can obviously be influenced by the choice of the input photon PDF. Thus the analysis is restricted to direct photoproduction, defined such that all data points satisfy $x_\gamma^{OBS} > 0.75$, where $x_\gamma^{OBS}$ is a measure of the fraction of the photon's momentum which enters into the hard scattering, see ref. [26]. This minimizes sensitivity to the choice of the photon PDF. The AFG photon PDF [29] is used to make the standard predictions, and the GRV photon PDF [30, 31] is used as a cross-check. There is no visible difference in the extracted proton PDFs.

The jet data are input to fits in which the $p_3$ and the $p_4$ parameters, which control the high-$x$ behaviour of the sea and the gluon PDF, are freed. It is found that these data constrain the gluon distribution in the range $0.01 \lesssim x \lesssim 0.1$. However, the sea distribution is not significantly constrained, so that the strategy of fixing one of the high-$x$ sea parameters is retained. Thus the ZEUS-JETS fit has 11 free parameters. The fit $\chi^2$ is 470 for 577 data points. The quality of the fit to the jet cross-sections is illustrated in Fig 4.

Fig. 5 compares the gluon distribution and its errors for 11 parameter fits including and not including the jet data. Although the jet data constrain the gluon directly only in the range $0.01 \lesssim x \lesssim 0.1$, the momentum sum-rule ensures that the indirect constraint of this data is still significant at higher $x$. The decrease in the uncertainty on the gluon distribution is striking, even up to high $Q^2$.

The shapes of the gluons from the ZEUS-O and the ZEUS-JETS fits are very similar as illustrated in the top plot of Fig. 6. This plot also shows that the valence and sea PDFs are not significantly influenced by the input of the jet data. The PDFs from the previous ZEUS-S global PDF analysis [14] and the MRST [11, 12] and CTEQ PDFs [13] are also shown on this figure. There is good agreement between all the ZEUS PDF extractions. The MRST and CTEQ PDFs are compatible with the ZEUS PDFs considering the size of the uncertainties on the PDFs. The bottom plot of Fig. 6 shows the ZEUS-JETS PDFs compared to those of H1 [32]. The shapes of the ZEUS and H1 gluons are different even though they are compatible considering the size of the uncertainties on each PDF extraction. Note that the Hessian method of treatment of the correlated systematic uncertainties used in the H1 fit results in a small estimate of experimental uncertainty on the gluon PDF, but the model uncertainty is significant. By contrast, the Offset method of treatment of correlated systematic uncertainties used in the ZEUS fit results in a larger estimate of experimental uncertainty which dominates the model uncertainty such that it is not visible.

### 3.3 ZEUS-JETS-$\alpha_s$ fit results

The conditions for this fit are the same as for the ZEUS-JETS fit, but $\alpha_s(M_Z^2)$ is a free parameter of the fit. The value

$$\alpha_s(M_Z^2) = 0.1183 \pm 0.0007(\text{uncorr.}) \pm 0.0018(\text{corr.}) \pm 0.0020(\text{norm.}) \pm 0.0008(\text{model})$$

is obtained, where the four uncertainties arise from the following: statistical and other uncorrelated sources; experimental correlated systematic sources excluding normalization uncertainties; normalization uncertainties; model uncertainty. Note that the uncertainty in $\alpha_s(M_Z^2)$ which usually comes from the correlation to the PDF shapes is automatically included in the experimental uncertainties. The model uncertainty has been evaluated by

- varying the value of $Q_0^2$ in the range $4 < Q_0^2 < 10$ GeV$^2$;
- varying the input parametrization by introducing $\sqrt{x}$ terms in the bracket $(1 + p_4 x)$ for the valence parametrizations and varying the choice of constraints applied to the sea parametrization as explained in Sec. 2;
- varying the cuts applied to the data entering the fit, in particular, there are small discrepancies between the fit predictions and jet data at the lowest transverse energies (this is also the case for the MRST and CTEQ PDFs [25, 26]), so the minimum tansverse energies of data entering the fit have been raised to $E_T^B > 10$ GeV and $E_T^{jet1} > 15$ GeV for DIS jets and photoproduced jets, respectively.

This is an NLO extraction. A crude estimate of the effect of terms beyond NLO can be made by variation of the choice of $\mu_R$. This scale has been varied by a factor of two for both the DIS jets and the photoproduced jets and additionally the conventional scale $\mu_R = Q$ for the inclusive cross-section data has been varied. The most significant effect comes from the variation of the scale for the photoproduction process. These scale changes produced shifts $\Delta\alpha_s(M_Z^2) \sim \pm 0.005$. Fig. 7 compares the present determination of $\alpha_s(M_Z^2)$ to other determinations from HERA and to the world average.

The extracted value of $\alpha_s(M_Z^2)$ is sufficiently close to the fixed value used in the ZEUS-JETS fit that there are no significant changes in the PDF parameters, but the correlation between $\alpha_s(M_Z^2)$ and the gluon PDF parameters increases the uncertainty on the gluon PDF as illustrated in Fig 8. The uncertainty on $\alpha_s(M_Z^2)$ is now so much less than that determined in the previous ZEUS-S analysis [14] that the total uncertainty on the gluon, including the uncertainty due to $\alpha_s(M_Z^2)$, is reduced in comparison to the total gluon uncertainty determined in the ZEUS-S global fit.

# 4 Summary

It is now possible to make a PDF fit within a single experiment with minimal external input, since ZEUS high-$Q^2$ cross-sections can now be used to constrain the valence PDFs and ZEUS low-$Q^2$ NC data can be used to constrain the low-$x$ sea and gluon distributions. Furthermore ZEUS data on jet production can be used to constrain the mid to high-$x$ gluon. This provides a compelling test of QCD factorization showing that NLO QCD is able to simultaneously describe inclusive cross-sections and jet cross-sections.

The constraint on the gluon PDF from the jet production data allows an accurate extraction of the value of $\alpha_s(M_Z^2)$,

$$\alpha_s(M_Z^2) = 0.1183 \pm 0.0028(\text{exp}) \pm 0.0008(\text{model}).$$

This is an NLO extraction. The uncertainty in $\alpha_s(M_Z^2)$ due to terms beyond NLO has been estimated as $\Delta\alpha_s(M_Z^2) \sim \pm 0.005$, by variation of the choice of renormalization scales.

The total uncertainty on the gluon PDF is reduced in comparison to the ZEUS-S global fit, because of the greater precision of the $\alpha_s(M_Z^2)$ measurement. The uncertainties on the valence PDFs are becoming competitive with those of the global fits and they are not subject to uncertainties from heavy target corrections. The precision of PDFs extracted from the global fits is now limited by the systematic errors of the contributing experiments, whereas the precision of the present ZEUS alone fit is still statistics limited, such that further improvement can be expected when higher precision HERA-II data are available.

# References


[1] ZEUS Coll., S. Chekanov *et al.* , Eur. Phys. J. **C 21**, 443 (2001).

[2] ZEUS Coll., J. Breitweg *et al.* , Eur. Phys. J. **C 12**, 411 (2000).

[3] ZEUS Coll., S. Chekanov *et al.* , Eur. Phys. J. **C 28**, 175 (2003).

[4] ZEUS Coll., S. Chekanov et al., Phys. Lett. **B 539**, 197 (2002).

[5] ZEUS Coll., S. Chekanov *et al.* , Preprint DESY-03-214 (hep-ex/0401003), DESY, 2004. Subm. to Phys. Rev. D.

[6] ZEUS Coll., S. Chekanov *et al.* , Eur. Phys. J. **C 32**, 16 (2003).

[7] V.N. Gribov and L.N. Lipatov, Sov. J. Nucl. Phys. **15**, 438 (1972).

[8] L.N. Lipatov, Sov. J. Nucl. Phys. **20**, 94 (1975).

[9] G. Altarelli and G. Parisi, Nucl. Phys. **B 126**, 298 (1977).

[10] Yu.L. Dokshitzer, Sov. Phys. JETP **46**, 641 (1977).

[11] A.D. Martin *et al.* , Eur. Phys. J. **C**, 73 (2002).

[12] A.D. Martin *et al.* , Eur. Phys. J. **C**, 455 (2002).

[13] J. Pumplin *et al.* , JHEP **0207**, 012 (2002).

[14] ZEUS Coll., S. Chekanov *et al.* , Phys. Rev. **D 67**, 012007 (2003).

[15] A.M. Cooper-Sarkar *et al.* , J. Phys. **G 25**, 1387 (1999).

[16] R.G. Roberts and R.S. Thorne, Phys. Rev. **D 57**, 6871 (1998).

[17] R.C.E. Devenish and A.M. Cooper-Sarkar, *Deep-Inelastic Scattering.* OUP, Oxford, UK, 2004.

[18] R.S. Towell *et al.* , Phys. Rev. **D 64**, 052002 (2002).

[19] P. Amaudruz *et al.* , Phys. Lett. **B 295**, 159 (1992).

[20] P. Amaudruz *et al.* , Phys. Rev. Lett. **66**, 2712 (1991).

[21] CCFR Coll., A.O. Bazarko *et al.* , Z. Phys. **C 65**, 189 (1995).

[22] Particle Data Group, S. Eidelman *et al.* , Phys. Lett. **B 592**, 1 (2004).

[23] A.M. Cooper-Sarkar, J. Phys. **G 28**, 2609 (2002).

[24] R.S. Thorne *et al.* , J. Phys. **G 28**, 2717 (2002).

[25] ZEUS Coll., S. Chekanov *et al.* , Phys. Lett. **B 547**, 164 (2002).

[26] ZEUS Coll., S. Chekanov *et al.* , Eur. Phys. J. **C 23**, 615 (2002).

[27] S. Frixione and G. Ridolfi, Nucl. Phys. **B 507**, 315 (1997).

[28] S. Frixione and M.H. Seymour, Nucl. Phys. **B 485**, 291 (1997).

[29] P. Aurenche, J.P. Guillet and M. Fontannaz, Z. Phys. **C 64**, 621 (1994).

[30] M. Glück, E. Reya and A. Vogt, Phys. Rev. **D 45**, 3986 (1992).

[31] M. Glück, E. Reya and A. Vogt, Phys. Rev. **D 46**, 1973 (1992).

[32] H1 Coll., C. Adloff *et al.* , Eur. Phys. J. **C 30**, 1 (2003).

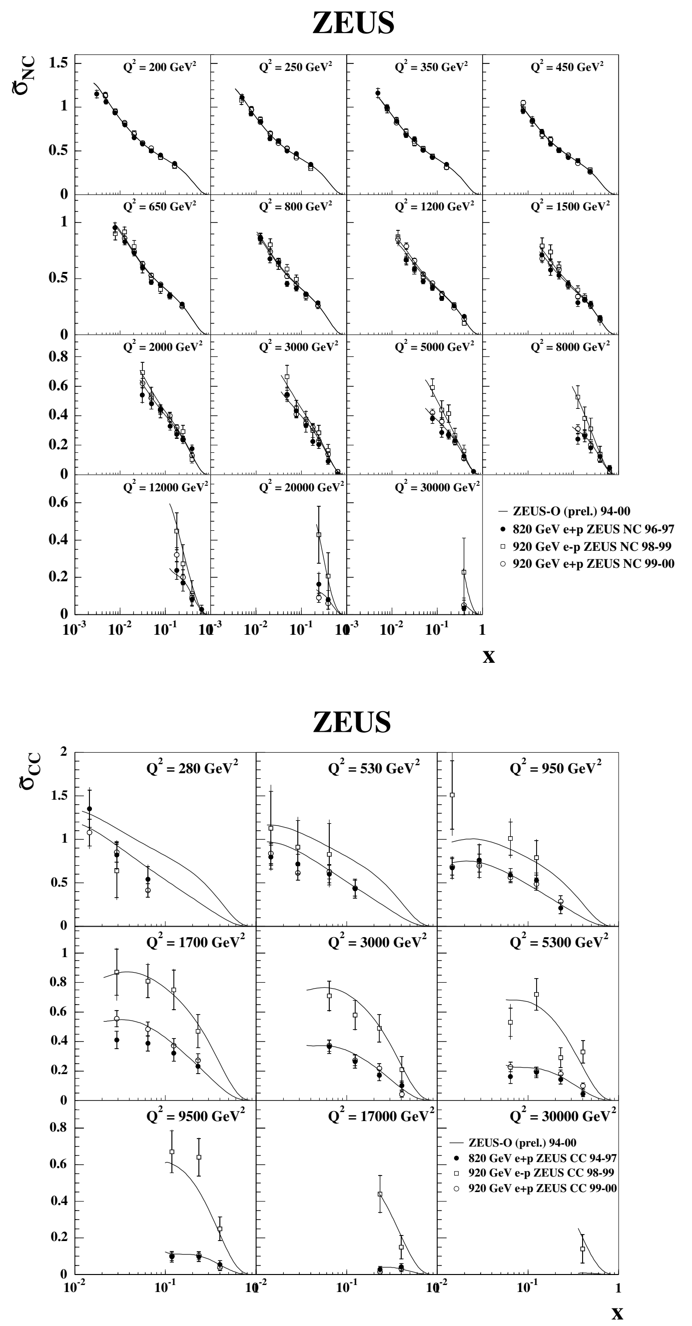


**Figure 1:** *Top plot: ZEUS-O fit to ZEUS high $Q^2$ NC data. Bottom plot: ZEUS-O fit to ZEUS high $Q^2$ CC data.*

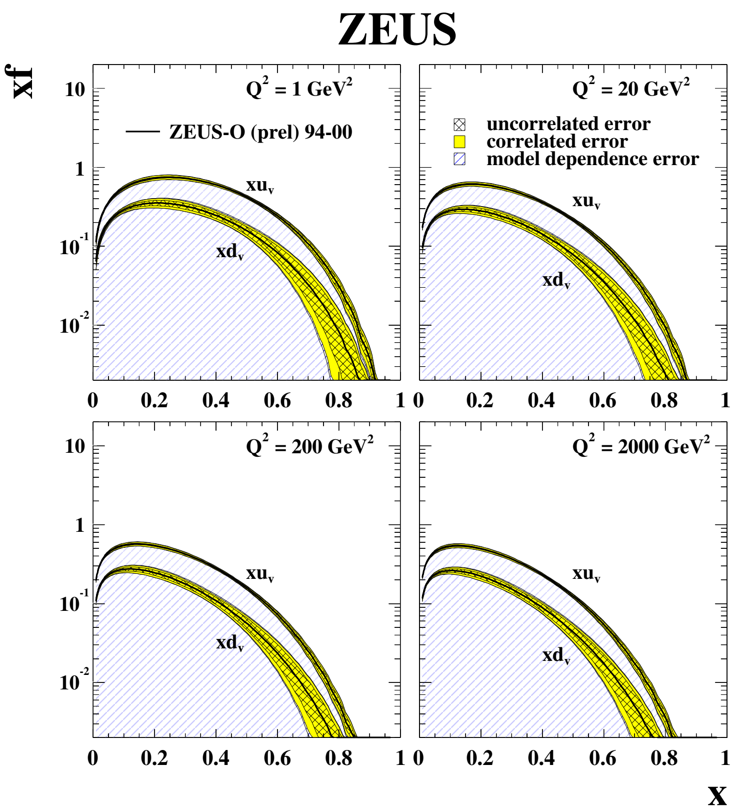


**Figure 2:** *Valence PDFs extracted from the ZEUS-O fit. The inner cross-hatched error bands show the statistical and uncorrelated systematic uncertainty, the middle grey error bands show the total experimental uncertainty including correlated systematic errors and normalizations and the outer hatched error bands show the model uncertainty.*

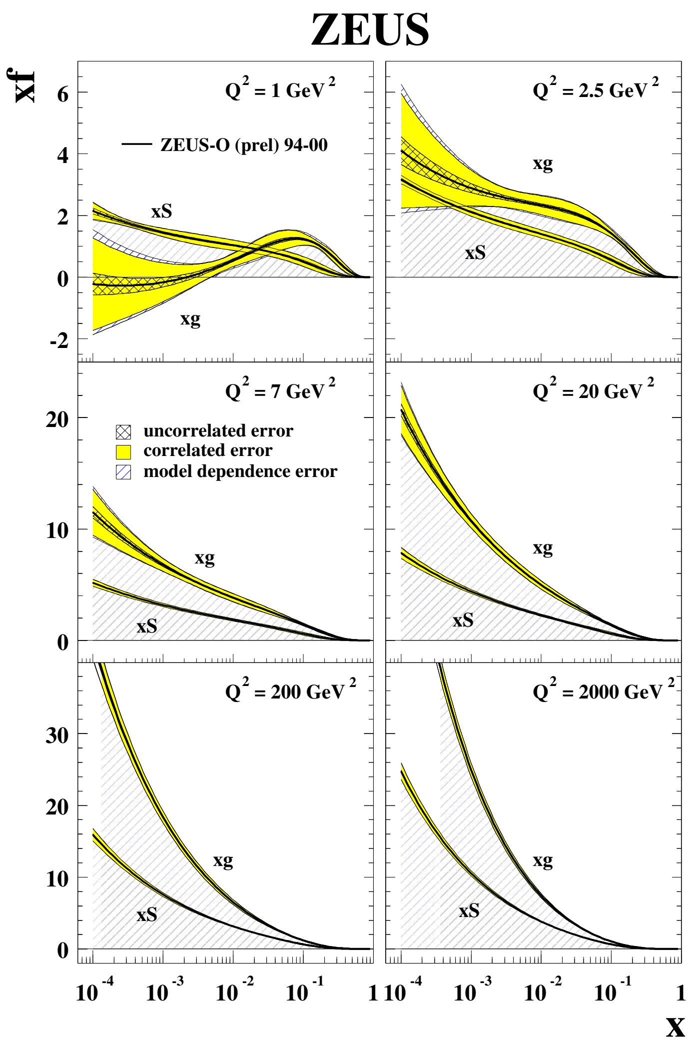


**Figure 3:** *Gluon and sea PDFs extracted from the ZEUS-O fit. The error bands are defined in the caption to Fig. 2*

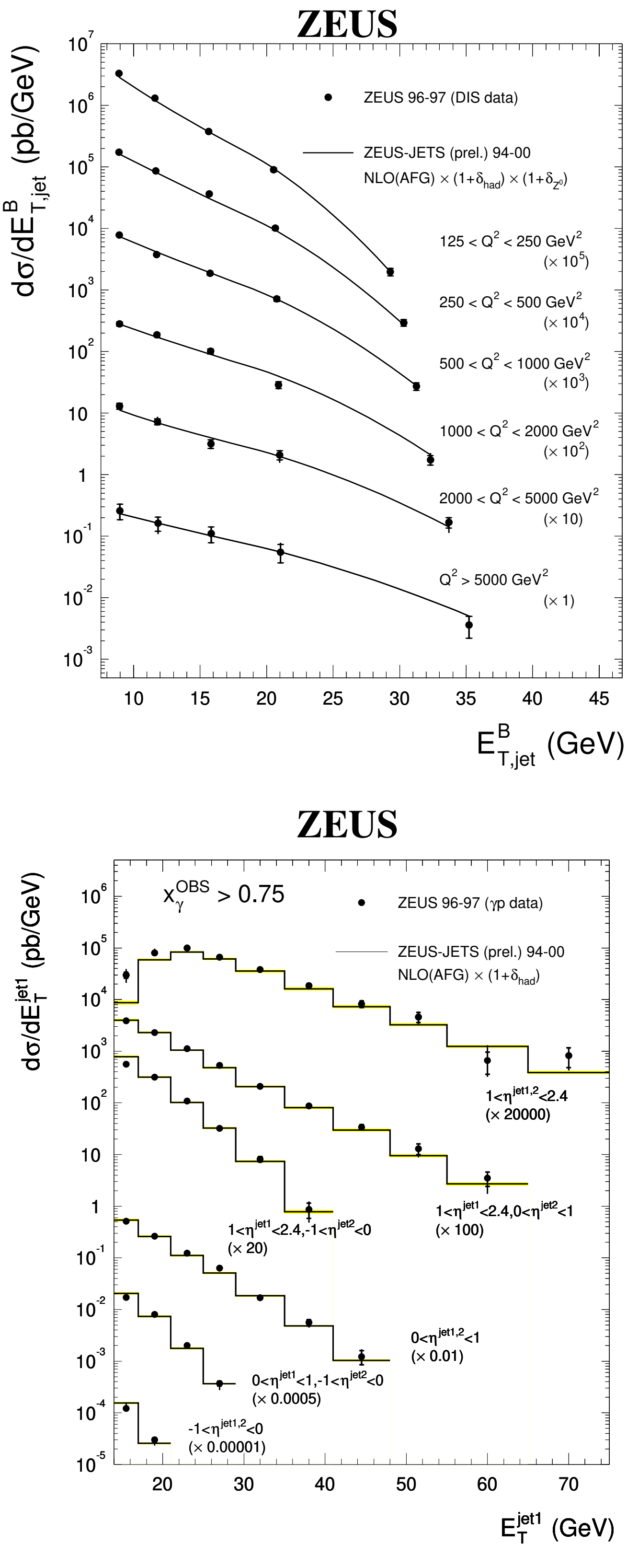


**Figure 4:** *Top plot: ZEUS-JETS fit compared to ZEUS DIS jet data. Bottom plot: ZEUS-JETS fit compared to direct photo-produced dijet data.*

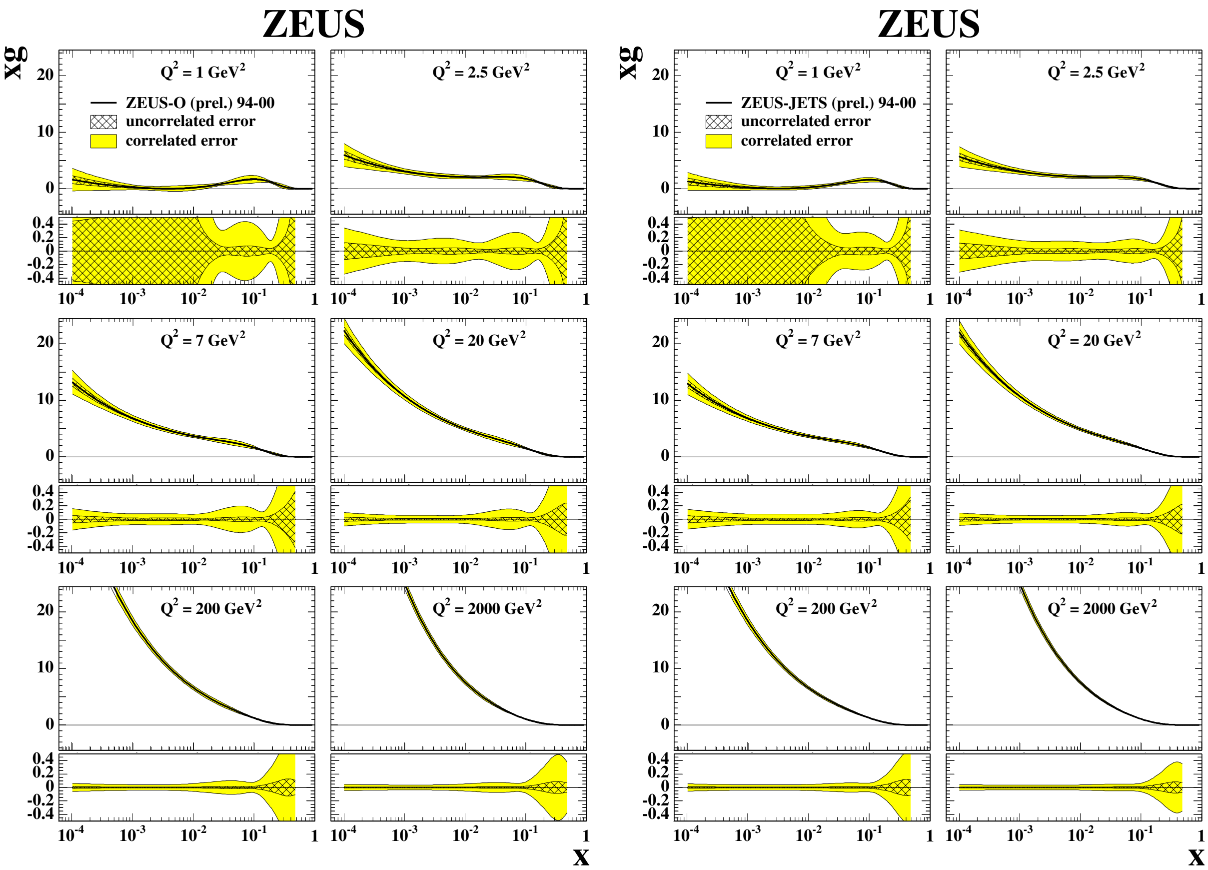


**Figure 5:** *Left plot: Gluon distributions extracted from an 11-parameter PDF fit excluding jet production data. Right plot: Gluon distributions extracted from an 11-parameter PDF fit including jet production data (ZEUS-JETS fit). The uncertainties on these distributions are shown beneath each distribution as fractional differences from the central value. The error bands are defined in the caption to Fig. 2. Note that model uncertainty is not visible for these fits.*

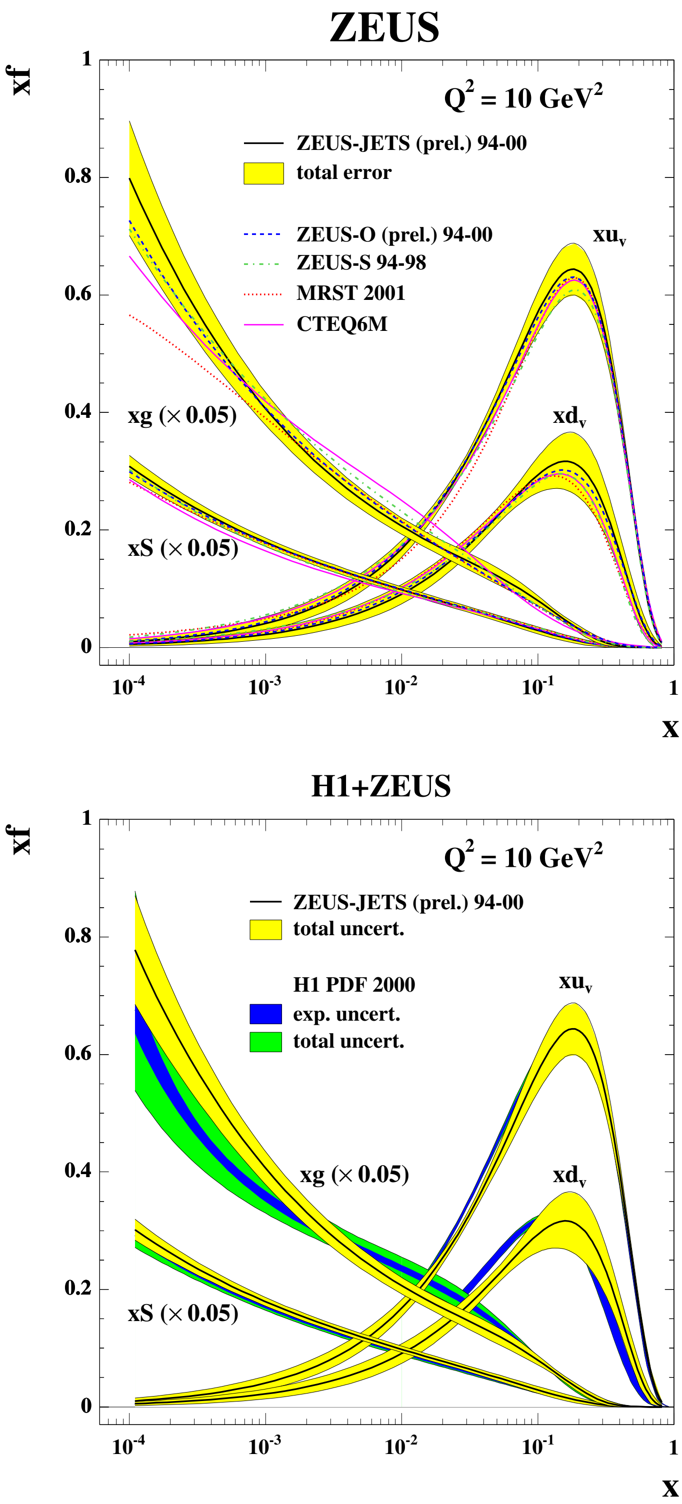


**Figure 6:** *Top plot: PDFs extracted from the new ZEUS-O and ZEUS-JETS fits compared to the previous ZEUS-S global analysis and to the MRST and CTEQ PDFs. Bottom plot: PDFs extracted from the ZEUS-JETS fit compared to the H1 2000 PDF analysis. Note that model uncertainty is not visible for the ZEUS-JETS fit.*

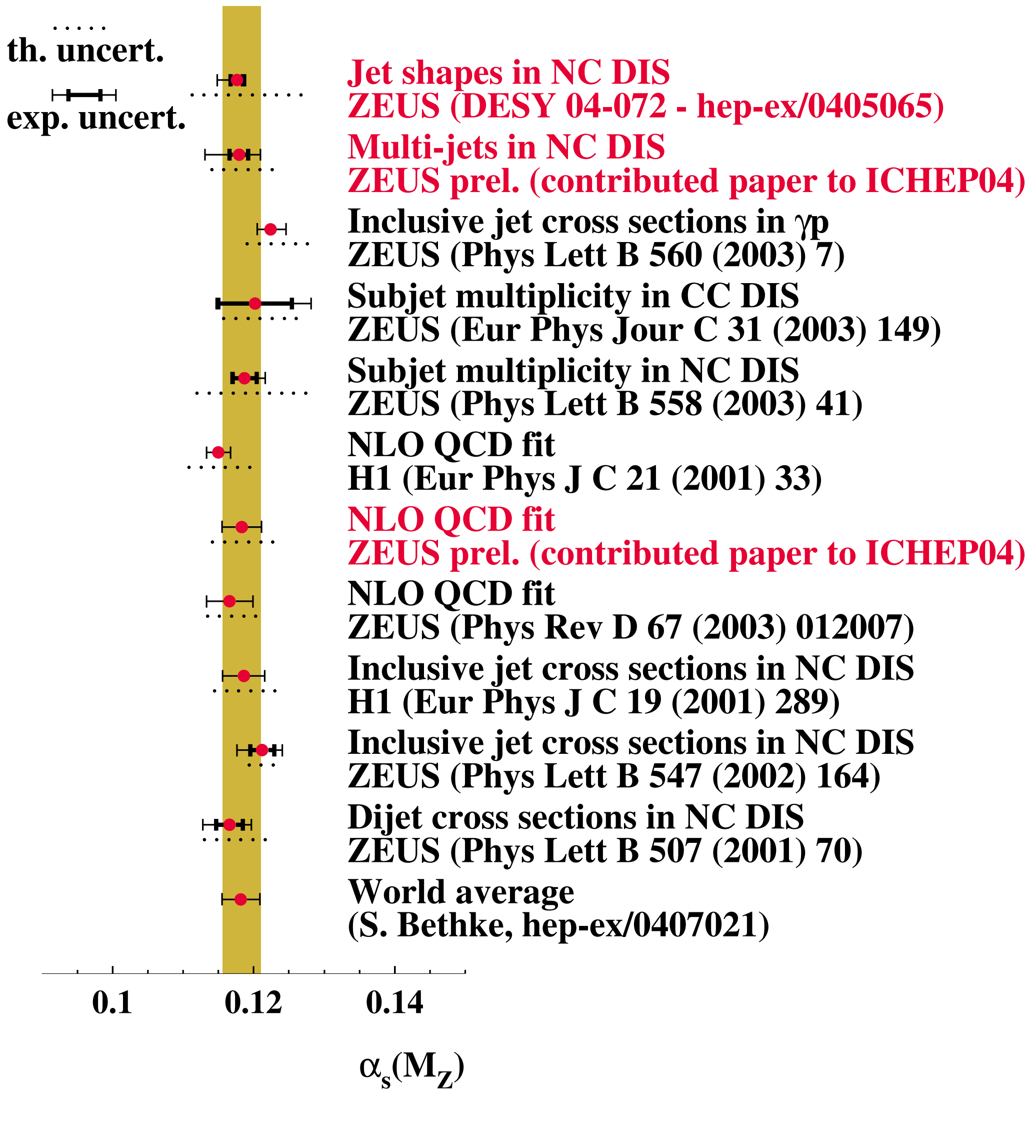


**Figure 7:** *Comparison of the present determination of $\alpha_s(M_Z^2)$ (NLO QCD fit ZEUS prel.) to other HERA determinations and to the world average.*

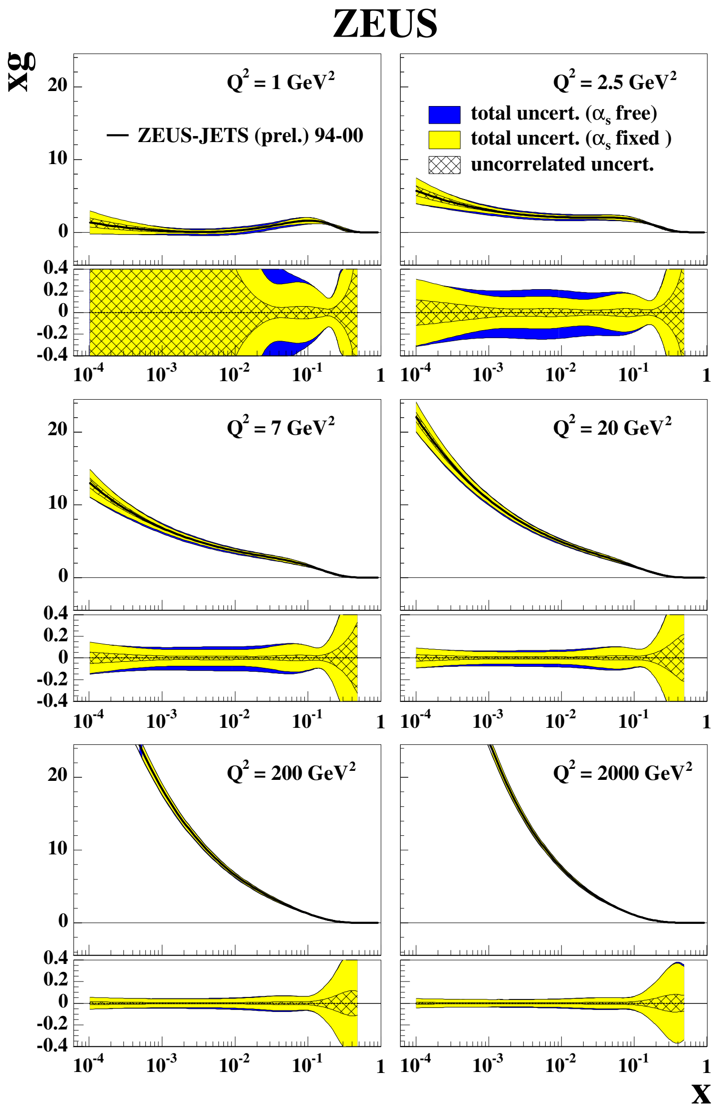


**Figure 8:** *Gluon distributions extracted from the ZEUS-JETS-$\alpha_s$ fit. The inner cross-hatched error bands show the statistical and uncorrelated systematic uncertainty, the middle grey error bands show the total experimental uncertainty including correlated systematic errors and normalizations and the outer cross-hatched error bands show the additional uncertainty in the gluon coming from the variation of $\alpha_s(M_Z^2)$. Model uncertainty is not visible for this fit.*